Arc eruptions deliver ‘first blow’ in the pulsed end-Permian mass extinction

Timothy Chapman (Timothy.Chapman@une.edu.au)
University of New England https://orcid.org/0000-0002-4821-6420
Luke Milan
University of New England https://orcid.org/0000-0003-3996-0992
Ian Metcalfe
University of New England https://orcid.org/0000-0003-3538-1686
Phil Blevin
Geological Survey of NSW
James Crowley
Boise State University

Article

Keywords: arc eruptions, Permian mass extinction event, flare-ups

Posted Date: November 12th, 2021

DOI: https://doi.org/10.21203/rs.3.rs-105487/v1

Abstract

Brief pulses of intense magmatic activity (flare-ups) along convergent margins represent drivers for climatic excursions that can lead to major extinction events. However, correlating volcanic outpouring to environmental crises in the geological past is often difficult due to poor preservation of volcanic sequences. Herein, we present a high-fidelity, CA-TIMS U–Pb zircon record of an end-Permian flare-up event in Eastern Australia, that involved the eruption of >39,000–150,000 km3 of silicic magma in c. 4.21 million years. A correlated high-resolution tephra record (c. 260–249 Ma) in the proximal sedimentary basins suggests recurrence of eruptions from the volcanic field in intervals of ~51,000–145,000 years. Peak eruption activity at 253 Ma is chronologically associated with the pulsed stages of the Permian mass extinction event. The ferocity of the 253 Ma eruption cycle in Eastern Australia is identified as a driver of greenhouse crises and ecosystem stress that led to the reduction in diversity of genera and the demise of the Glossopteris Forests. Simultaneous global continental margin arc flare-up events could thus present an additional agent to trigger greenhouse warming and ecosystem stress that preceded the catastrophic eruption of the Siberian Traps.

Full Text

Extinction events in Earth's history are associated with perturbations in climate. The triggers are typically related to bolide impacts or vast outpouring from large igneous provinces[1-3]. The largest extinction at the end of the Permian Period, accounting for the loss of up to 85–90% of marine invertebrates and 75% of terrestrial species, is inferred to be caused by the eruption of the Siberian Traps[2-5]. Although, additional drivers including methane release from clathrates, hypercapnia, oceanic anoxia and acidification have been suggested as causative to the end-Permian extinction event (see discussion in[4]). Coincidental periods of heightened arc volcanism can also lead to significant greenhouse aerosol emission (H_2O, CO_2, and CH_4: Fig. 1) that are often greater than basaltic eruptions due to interactions with crust rich in carbonate and carbonaceous material[6-10]. The resulting climatic variability could feasibly contribute to extinction events locally or globally, depending on the scale of the eruptions[7].

Despite continuous and long-lived subduction, the volumetric input of magma into volcanic arcs is highly episodic[7,11]. Magmatic flare-up events of *c.* 2 to 20 million years are interspersed by longer periods of relative quiescence (spanning ~30–70 million years)[12]. These flare-up periods can be a global phenomenon (Fig. 1)[6]. The magmatic addition in a flare-up can be as much as 10 to 1000 times greater than in a steady-state (per km length of arc every million years)[13]. It is less clear how these volumetric addition rates correlate to the volcanic record, where preservation is poor. Studies from young volcanic arcs suggest cycles of large outbursts of silicic eruptions occur with shorter periodicities (Kyr to a few Myr) within these broader flare-up periods[14,15].

Relatively few volcanic arcs preserve direct evidence linking eruptions to particular flare-up cycles[16], let alone to periods of climatic perturbations or extinction[6,7]. As volcanic arcs account for most

silicic eruptions on the planet and can attribute appreciable outpouring of gases (CO_2, H_2O and CH_4)[6,7,9], understanding their periodicity and eruption volume is of crucial importance. This is particularly so during periods of global climatic and environmental instability, such as at the end of the Permian.

Eastern Australia Permian flare-up

A high-fidelity record of arc magmatism is presented from the Permian to Triassic margin in Eastern Australia (Figs 1 & 2). New high-precision Chemical Abrasion Isotope Dilution Thermal Ionisation Mass Spectrometry (CA-TIMS) U–Pb zircon ages were measured on nine volcanic deposits and three representative coeval granites. The weighted mean $^{206}Pb/^{238}U$ CA-TIMS dates were obtained from analyses composed of populations of single zircon grains, initially screened using cathodoluminescence imaging for magmatic grains that lack inherited cores. The results are combined with published CA-TIMS ages on 73 tephra in adjacent sedimentary basins and 128 SHRIMP/LA-ICPMS ages on granites of the New England Batholith[17]. The age systematics are compiled with geological mapping[18-20] and estimates of crustal thickness based on Sr/Y trends to quantify the scale of magmatism for the first time.

Two major flare-up cycles are identified along the arc at *c.* 290–280 Ma (30 km^3/my per km) and *c.* 260–245 Ma (63 km^3/my per km) that punctuate the background low-volume magmatism along the margin (5–10 km^3/my per km: Fig. 3)[21]. The *c.* 290–280 Ma peak is related to back-arc extension and crustal reworking[22]. The Permian–Triassic event is associated with increasing mantle input to form the prominent batholith[23]. A voluminous sequence (Fig 3) of silicic ignimbrite sheets totalling thicknesses of 6.5–8 km is also preserved at this time over a broad surface expression supporting the estimated high magma fluxes[18-20]. The deposits are consistent with a ratio of volcanic to plutonic material of 1:1 to 1:14. It is less clear how representative the higher than typical ratios observed in arcs (1:2 to 1:30)[12] are in the context of preservation of igneous rock. However, the ratios are consistent with inferences from modern extending arcs[14] that preserve thick piles of volcanic strata in a setting similar to that of Eastern Australia in the Permian (Fig. 3a).

The volcanic field preserves 4–8 distinct calderas which span an eruption period of *c.* 257.54 to 253.34 Ma (Fig. 2). The thickness of each volcanic member varies between 500–4000 m based on mapped relationships or geophysical observations[18-20]. The distribution is consistent with the eruption of at least 39,000 km^3 from three centres that migrated over time (Fig. 2). Initial volcanism occurred in the Western Belt involving ~22,750 km^3 of caldera infill over *c.* 2.06 Myr (*c.* 257.54–255.48 Ma), before tracking to the Southern Belt to erupt ~3,250 km^3 over *c.* 1.12 Myr (*c.* 255.7–254.58 Ma), and then further to the northeast (Eastern Belt) where multiple large eruptions (~13,000 km^3) occurred over the shortest interval of *c.* 0.49 Myr (*c.* 253.59–253.1 Ma). Voluminous granitic magmatism follows a similar spatial and temporal trend and persisted in the region until *c.* 242 Ma[17,22], including as resurgent feeder dykes that define the calderas (Fig. 2)[18].

The structural relationships of the ignimbrite sequence (Fig. 2) are consistent with it being draped over an undulating topography, with erosion of the pile or the volcanic detritus occurring between individual eruptions[18,19]. Most of the overburden to the youngest volcanic end-members appears to have been lost, consistent with predictions of ~3–4 km of denudation on the New England Tablelands in the last 100 million-years[24]. The volcanic deposits are also truncated in their original extent in all cardinal directions by dissection of the New England Tableland, particularly along the Great Escarpment to the east and the Peel Fault to the south and west (Fig. 2)[22]. Together these relationships suggest that the preserved volcanic material only records part of the duration of volcanism and is a minimum estimate for the eruption volume. Based solely on the preserved aerial extent of deposits across the entire volcanic field, the eruption volume of the Wandsworth Volcanic Group is 150,000 km^3 (Fig. 2a). Although, this estimate does not account for the ~3–4 km of erosion and the amount of ash or other eruptive material that was not preserved near the primary volcanic centres, or in the adjacent Permian basins.

Sedimentary basins proximal to the volcanic field preserve up to 250 tephra spanning the *c.* 260–247 Ma time frame supporting extensive volcanic outburst during the flare-up event (Figs 2 & 4)[25-29]. The compilation of tephra intervals in the Sydney, Gunnedah, Bowen, and Galilee Basins are consistent with the recurrence of eruptions every ~51,000–145,000 years with an increase in activity at *c.* 253 Ma (Figs 3b & 4). The total volumetric output from the tephra is less certain, but high-density layers at *c.* 254–252 Ma have total thicknesses of >100 m across the entire Sydney and Bowen Basin (60,000–64,000 km^2 each)[25,27]. Geochemical fingerprints of these events are consistent with contiguous and prolonged volcanism from the same, or similar rhyodacite to rhyolite sources that match those identified in the New England region[30,31]. The large dispersive extent of tephra and their general thicknesses is consistent with super-eruptions blanketing the majority of Eastern Australia in ash-fall and debris over an area of at least 950,000 km^2 consistent with eruptions volumes of >150,000 km^3 (Fig. 2).

Sources of silicic eruptions

The only prominent local source of silicic ash in Eastern Australia is the temporally correlated Wandsworth Volcanic Group and their spatially associated granites in the southern New England Orogen. Although, along arc extensions in northern Queensland are inferred to be additional contributors, particularly into the Bowen and Galilee basins, they lack prominent exposed volcanic sequences due to partial or complete erosion[32]. The high proportion of tephra layers at ~253–254 Ma corresponds to the vast outpouring of the Eastern Belt. The Dundee Rhyodacite, one of the largest ignimbrite deposits preserved today (~918 km^2), can be correlated to individual tephra of the thick Awaba Tuff (>11 m thick: *c.* 253.1 Ma) and its regionally extensive correlatives throughout the other sedimentary basins in eastern Australia[25-27,31]. The slightly younger Yarrabee Tuff (dated at *c.* 252.54–253.07 Ma)[25,26,31] in the Bowen and Galilee basin and the Garie Tuff in the Sydney basin (*c.* 247.87 and 248.23) have been linked to the later stages of eruption from the Eastern volcanic belt, but lack an ignimbrite deposit, likely due to subsequent erosion[31]. The prominence of resurgent granitic magmatism around the Eastern Belt and the

occurrence of thick ignimbrite deposits (Emmaville and Dundee) is consistent with this region representing the key focal point of magmatism that spanned the end-Permian interval (Fig. 2).

A second period of higher-density tephra preservation occurs at 255 and 257 Ma in the surrounding Permian sedimentary basins. These ash layers match the ages of the ignimbrite deposits from the Southern and Western Belt of the Wandsworth Volcanic Group (Fig. 4). The volcanic events are less extensive in the tephra-record and are mostly focused in the Gunnedah, Sydney and southern portions of the Bowen basins suggesting a sustain period (*c.* 2 Myr) of high-volume eruptions[25,31].

Globally, the commonality of arc magmatism at the end of the Permian is consistent with similar eruption-styles occurring concurrently along the margins of the supercontinent Pangea[7,8]. Synchronous flare-up peaks at *c.* 255–250 Ma have been identified throughout South America, Antarctica, and China (Fig. 1)[33-36]. These include the estimated $1.3x10^6$ km^3 of silicic volcanism from the Choiyoi province in South America and Antarctica that is inferred to have contributed to greenhouse warming near the end-Guadalupian event[34]. Altogether global arc volcanism at the end of the Permian Period would have increased the total volcanic gas output, including the heightened production of greenhouse gasses[7,8].

Super-eruptions and the end-Permian extinction

The end-Permian mass extinction is inferred to have transpired in several pulses[37-39], plausibly initiated by a series of climatic perturbations preceding the actual Permian–Triassic boundary currently dated at 251.90 ± 0.10 Ma (Fig. 4)[40,41]. The eruption of extensive flood basalts as part of the Siberian Traps is considered to have had the greatest influence on climatic perturbations during the period of *c.* 252.3–251.9 Ma (Fig. 4)[3,4]. However, it has been argued that multiple causative agents contributed to the periodic demise of biota and the reduction of diversity from *c.* 258 until 254 Ma (Fig. 4)[442]. Particularly since the onset of the late Permian warming (*c.* 254 Ma) occurred prior to the eruption of the Siberian Traps[38,43-46].

Many terrestrial basins in the Southern Hemisphere (*c.* 252.5 Ma)[47], have less severe extinction events before the delineated end Permian extinction horizon (Fig. 4)[28,48-51]. A series of greenhouse crises have been identified from palynological and geochemical proxies in the high-latitude Sydney Basin, consistent with a period of climatic variability from *c.* 265 Ma to the beginning of the Triassic (Fig. 4)[48,52,53]. The Eastern Australia flare-up, and the along-strike extensions throughout Pangea present as compelling agents to some of these cycles of greenhouse conditions[54] (Figs 1 & 4). Although, until now the precise timing, vast quantitative scale, and extent of these eruptions in Eastern Australia has remained speculative.

Eruptions in Eastern Australia peaked at *c.* 254–252.5 Ma, corresponding to a negative excursion in local carbon isotopic ratios (Fig. 4)[25]. This event marks the initiation of multiple end-Permian greenhouse crises (Fig. 4), involving perturbations in temperature, atmospheric CO_2 and rainfall in eastern

Australia[52]. The ultra-Plinian (>1000 km^3) eruptions of the Emmaville (Fassifern Tuff), Dundee (Awaba Tuff) and the Yarrabee Tuff directly correspond temporally to identified greenhouse crises[52,55], all of which pre date the Siberian Traps and the penultimate end Permian extinction. Additional Triassic greenhouse crises correspond to renewed volcanism associated to the Garie Tuff (Fig. 3b).

Multiple local environmental crises are likely to have been exacerbated by both the short- and longer-term consequences of catastrophic eruptions. These would include the initial cooling associated with the albedo effect of ash, followed by the prolonged greenhouse forcing related to the vast emission of volcanic aerosols[10]. Extensive drought, forest fires and higher atmospheric carbon are inferred at this time based on pollen records from the intervening sedimentary layers to the tephra that correspond to the volcanic sequence (Fig. 3b)[28]. Generally, the *c.* 254–252 Ma period marks a significant change from cold glaciated conditions to progressive warming in Australia as well as globally (Fig. 4)[28,37,39,44,45,49-51]. In particular, the pronounced increase in seasonal temperatures just before 252.54 Ma[47] is proposed to have led to the demise of the *Glossopteris* forests in Gondwana forming a prominent extinction horizon (Figs 3 & 4)[47,48].

The excellent geological record of flare-up in Eastern Australia provides a direct link between continental arc volcanism and localised records of ecosystem stress, beyond previously utilised stratigraphic coincidences[35]. The record from Eastern Australia is consistent with arc eruptions being influential to progressive species demise, but not the ultimate fatal blow. The synchronous pulse of arcs documented around Pangea at *c.* 252–260 Ma[33-36] is a likely contributor to inducing ecosystem collapse via warming[7,35,56] prior to the catastrophe at *c.* 251.9 Ma (Fig. 4). Volcanic outbursts present an under recognised contributor that can plausibly account for the temporal variability and pulsed nature of the end Permian mass extinction event, as well as others generally throughout Earth's past.

Declarations

Acknowledgements

T. C. acknowledges funding via the University of New England Postdoctoral Fellowship scheme and resources at the School of Environment and Rural Sciences. I. M. acknowledges funding provided by the Australian Research Council Grant DP109288. P. L. B. publishes with the permission of the ED of the Geological Survey of NSW. We appreciate helpful comments on the work provided by G. Clarke, K. Bull, J. Paterson, N. Campione, N. Daczko, and J. S. Lackey.

Author contributions

T. C, L. A. M., I. M and P. L. B initiated the project and contributed to the analysis of the data. J. C. completed the data collection and interpretation. All authors contributed to writing and reviewing the manuscript.

Competing Interests: The authors declare no competing interest

References

1. Courtillot, V. E. & Renne, P. R. On the ages of flood basalt events. *Comptes Rendus Geoscience* **335**, 113–140 (2003).
2. Campbell, I., Czamanske, G., Fedorenko, V., Hill, R. & Stepanov, V. Synchronism of the Siberian Traps and the Permian–Triassic boundary. *Science* **258**, 1760–1763 (1992).
3. Burgess, S. D. & Bowring, S. A. High-precision geochronology confirms voluminous magmatism before, during, and after Earth's most severe extinction. *Science advances* **1**, doi:e1500470 (2015).
4. Payne, J. L. & Clapham, M. E. End-Permian mass extinction in the oceans: an ancient analog for the twenty-first century? *Annual Review of Earth and Planetary Sciences* **40**, 89–111 (2012).
5. Schneebeli-Hermann, E. *et al.* Evidence for atmospheric carbon injection during the end-Permian extinction. *Geology* **41**, 579–582 (2013).
6. Lee, C. & Lackey, J. Global continental arc flare-ups and their relation to long-term greenhouse conditions. *Elements* **11**, 125–130 (2015).
7. McKenzie, N. R. *et al.* Continental arc volcanism as the principal driver of icehouse-greenhouse variability. *Science* **352**, 444–447 (2016).
8. Ratschbacher, B. C., Paterson, S. R. & Fischer, T. P. Spatial and depth-dependent variations in magma volume addition and addition rates to continental arcs: Application to global CO2 fluxes since 750 Ma. *Geochemistry, Geophysics, Geosystems* **20**, 2997–3018 (2019).
9. Soreghan, G. S., Soreghan, M. J. & Heavens, N. G. Explosive volcanism as a key driver of the late Paleozoic ice age. *Geology* **47**, 600–604 (2019).
10. Jones, M. T., Sparks, R. S. J. & Valdes, P. J. The climatic impact of supervolcanic ash blankets. *Climate Dynamics* **29**, 553–564 (2007).
11. DeCelles, P. G., Ducea, M. N., Kapp, P. & Zandt, G. Cyclicity in Cordilleran orogenic systems. *Nature Geoscience* **2**, 251–257 (2009).
12. Ducea, M. N., Paterson, S. R. & DeCelles, P. G. High-volume magmatic events in subduction systems. *Elements* **11**, 99–104 (2015).
13. Milan, L. A., Daczko, N. R. & Clarke, G. L. Cordillera Zealandia: A Mesozoic arc flare-up on the palaeo-Pacific Gondwana Margin. *Scientific Reports* **7**, 261, doi:10.1038/s41598-017-00347-w (2017).
14. Gravley, D. M., Deering, C. D., Leonard, G. S. & Rowland, J. V. Ignimbrite flare-ups and their drivers: A New Zealand perspective. *Earth-Science Reviews* **162**, 65–82, doi:https://doi.org/10.1016/j.earscirev.2016.09.007 (2016).
15. de Silva, S. L., Riggs, N. R. & Barth, A. P. Quickening the Pulse: Fractal Tempos in Continental Arc Magmatism. *Elements* **11**, 113–118, doi:10.2113/gselements.11.2.113 (2015).
16. Attia, S., Cottle, J. M. & Paterson, S. R. Erupted zircon record of continental crust formation during mantle driven arc flare-ups. *Geology* **48**, 446–451, doi:10.1130/g46991.1 (2020).

17. Chisholm, E.-K. I., Simpson, C. & Blevin, P. *New SHRIMP U–Pb Zircon Ages from the New England Orogen, New South Wales: July 2010-June 2012*. (Geoscience Australia, 2014).
18. McPhie, J. Evolution of a non-resurgent cauldron: the Late Permian Coombadjha Volcanic Complex, northeastern New South Wales, Australia. *Geological Magazine* **123**, 257–277 (1986).
19. Lackie, M. The magnetic fabric of the Late Permian Dundee Ignimbrite, Dundee, NSW. *Exploration Geophysics* **19**, 481–488 (1988).
20. Stewart, A. Facies in an Upper Permian volcanic succession, Emmaville Volcanics, Deepwater, northeastern New South Wales. *Australian Journal of Earth Sciences* **48**, 929–942 (2001).
21. Milan, L. A. *et al.* A New Reconstruction for Permian East Gondwana Based on Zircon Data From Ophiolite of the East Australian Great Serpentinite Belt. *Geophysical Research Letters* **48**, e2020GL090293, doi:https://doi.org/10.1029/2020GL090293 (2021).
22. Rosenbaum, G. The Tasmanides: Phanerozoic tectonic evolution of eastern Australia. *Annual Review of Earth and Planetary Sciences* **46**, 291–325 (2018).
23. Shaw, S., Flood, R. & Pearson, N. The New England Batholith of eastern Australia: Evidence of silicic magma mixing from zircon 176Hf/177Hf ratios. *Lithos* **126**, 115–126 (2011).
24. Kohn, B. *et al.* Shaping the Australian crust over the last 300 million years: insights from fission track thermotectonic imaging and denudation studies of key terranes. *Australian Journal of Earth Sciences* **49**, 697–717 (2002).
25. Metcalfe, I., Crowley, J., Nicoll, R. & Schmitz, M. High-precision U–Pb CA-TIMS calibration of Middle Permian to Lower Triassic sequences, mass extinction and extreme climate-change in eastern Australian Gondwana. *Gondwana Research* **28**, 61–81 (2015).
26. Laurie, J. *et al.* Calibrating the middle and late Permian palynostratigraphy of Australia to the geologic time-scale via U–Pb zircon CA-IDTIMS dating. *Australian Journal of Earth Sciences* **63**, 701–730 (2016).
27. Creech, M. Tuffaceous deposition in the Newcastle Coal Measures: challenging existing concepts of peat formation in the Sydney Basin, New South Wales, Australia. *International journal of coal geology* **51**, 185–214 (2002).
28. Vajda, V. *et al.* End-Permian (252 Mya) deforestation, wildfires and flooding—An ancient biotic crisis with lessons for the present. *Earth and Planetary Science Letters* **529**, 115875 (2020).
29. Frank, T. D. *et al.* Pace, magnitude, and nature of terrestrial climate change through the end-Permian extinction in southeastern Gondwana. *Geology*, doi:10.1130/g48795.1 (2021).
30. Grevenitz, P., Carr, P. & Hutton, A. Origin, alteration and geochemical correlation of Late Permian airfall tuffs in coal measures, Sydney Basin, Australia. *International Journal of Coal Geology* **55**, 27–46 (2003).
31. Phillips, L. *et al.* U–Pb geochronology and palynology from Lopingian (upper Permian) coal measure strata of the Galilee Basin, Queensland, Australia. *Australian Journal of Earth Sciences* **65**, 153–173 (2018).

32. Siégel, C., Bryan, S., Allen, C., Gust, D. & Purdy, D. Crustal evolution in the New England Orogen, Australia: repeated igneous activity and scale of magmatism govern the composition and isotopic character of the continental crust. *Journal of Petrology*, doi:org.ezproxy.une.edu.au/10.1093/petrology/egaa078 (2020).
33. Wang, X. *et al.* Convergent continental margin volcanic source for ash beds at the Permian-Triassic boundary, South China: Constraints from trace elements and Hf-isotopes. *Palaeogeography, Palaeoclimatology, Palaeoecology* **519**, 154–165 (2019).
34. Nelson, D. & Cottle, J. Tracking voluminous Permian volcanism of the Choiyoi Province into central Antarctica. *Lithosphere* **11**, 386–398 (2019).
35. He, B., Zhong, Y.-T., Xu, Y.-G. & Li, X.-H. Triggers of Permo-Triassic boundary mass extinction in South China: the Siberian Traps or Paleo-Tethys ignimbrite flare-up? *Lithos* **204**, 258–267 (2014).
36. Cope, T. Phanerozoic magmatic tempos of North China. *Earth and Planetary Science Letters* **468**, 1–10 (2017).
37. Sun, Y. *et al.* Lethally hot temperatures during the Early Triassic greenhouse. *Science* **338**, 366–370 (2012).
38. Jin, Y. *et al.* Pattern of marine mass extinction near the Permian-Triassic boundary in South China. *Science* **289**, 432–436 (2000).
39. Song, H., Wignall, P. B., Tong, J. & Yin, H. Two pulses of extinction during the Permian–Triassic crisis. *Nature Geoscience* **6**, 52–56 (2013).
40. Ramezani, J. & Bowring, S. A. Advances in numerical calibration of the Permian timescale based on radioisotopic geochronology. *Geological Society, London, Special Publications* **450**, 51–60 (2018).
41. Joachimski, M. M. *et al.* Climate warming in the latest Permian and the Permian–Triassic mass extinction. *Geology* **40**, 195–198 (2012).
42. Alroy, J. *et al.* Phanerozoic trends in the global diversity of marine invertebrates. *Science* **321**, 97–100 (2008).
43. Mundil, R., Ludwig, K. R., Metcalfe, I. & Renne, P. R. Age and timing of the Permian mass extinctions: U/Pb dating of closed-system zircons. *Science* **305**, 1760–1763 (2004).
44. Chen, B. *et al.* Permian ice volume and palaeoclimate history: oxygen isotope proxies revisited. *Gondwana Research* **24**, 77–89 (2013).
45. Shen, S. Z. *et al.* High-resolution Lopingian (Late Permian) timescale of south China. *Geological Journal* **45**, 122–134 (2010).
46. Shellnutt, J. G., Denyszyn, S. W. & Mundil, R. Precise age determination of mafic and felsic intrusive rocks from the Permian Emeishan large igneous province (SW China). *Gondwana Research* **22**, 118–126 (2012).
47. Fielding, C. R. *et al.* Sedimentology of the continental end-Permian extinction event in the Sydney Basin, eastern Australia. *Sedimentology* **68**, 30–62, doi:https://doi.org/10.1111/sed.12782 (2021).

48. Fielding, C. R. *et al.* Age and pattern of the southern high-latitude continental end-Permian extinction constrained by multiproxy analysis. *Nature communications* **10**, 1–12 (2019).
49. Liu, Z. *et al.* Osmium-isotope evidence for volcanism across the Wuchiapingian–Changhsingian boundary interval. *Chemical Geology* **529**, 119313 (2019).
50. Cheng, C. *et al.* Permian carbon isotope and clay mineral records from the Xikou section, Zhen'an, Shaanxi Province, central China: Climatological implications for the easternmost Paleo-Tethys. *Palaeogeography, Palaeoclimatology, Palaeoecology* **514**, 407–422 (2019).
51. Gastaldo, R. A. *et al.* The base of the Lystrosaurus Assemblage Zone, Karoo Basin, predates the end-Permian marine extinction. *Nature Communications* **11**, 1–8 (2020).
52. Retallack, G. J. *et al.* Multiple Early Triassic greenhouse crises impeded recovery from Late Permian mass extinction. *Palaeogeography, Palaeoclimatology, Palaeoecology* **308**, 233–251 (2011).
53. Mays, C. *et al.* Refined Permian–Triassic floristic timeline reveals early collapse and delayed recovery of south polar terrestrial ecosystems. *Bulletin* **132**, 1489–1513 (2020).
54. Yugan, J., Jing, Z. & Qinghua, S. Two phases of the end-Permian mass extinction. (1994).
55. Williams, M. L., Jones, B. G. & Carr, P. F. The interplay between massive volcanism and the local environment: Geochemistry of the Late Permian mass extinction across the Sydney Basin, Australia. *Gondwana Research* **51**, 149–169 (2017).
56. van der Boon, A. *et al.* Exploring a link between the Middle Eocene Climatic Optimum and Neotethys continental arc flare-up. *Clim. Past* **17**, 229–239, doi:10.5194/cp-17-229-2021 (2021).
57. Metcalfe, I. Tectonic evolution of Sundaland. *Bulletin of the Geological Society of Malaysia* **63**, 27–60 (2017).
58. Maravelis, A. G. *et al.* Re-assessing the Upper Permian Stratigraphic Succession of the Northern Sydney Basin, Australia, by CA-IDTIMS. *Geosciences* **10**, 474 (2020).
59. Voice, P. J., Kowalewski, M. & Eriksson, K. A. Quantifying the timing and rate of crustal evolution: global compilation of radiometrically dated detrital zircon grains. *The Journal of Geology* **119**, 109–126 (2011).

Figures

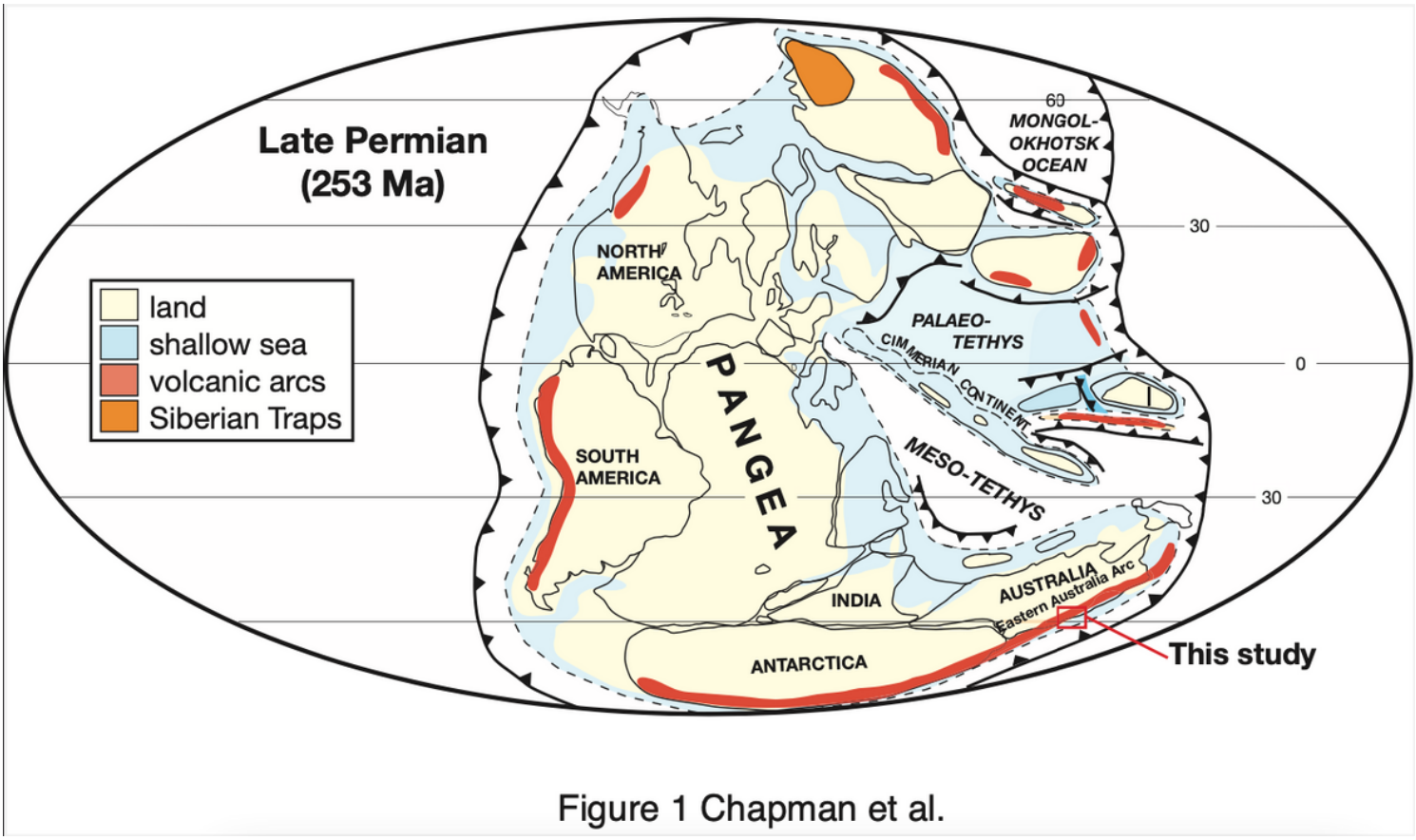

Figure 1

Global arc activity on the Pangea supercontinent at c. 253 Ma57.

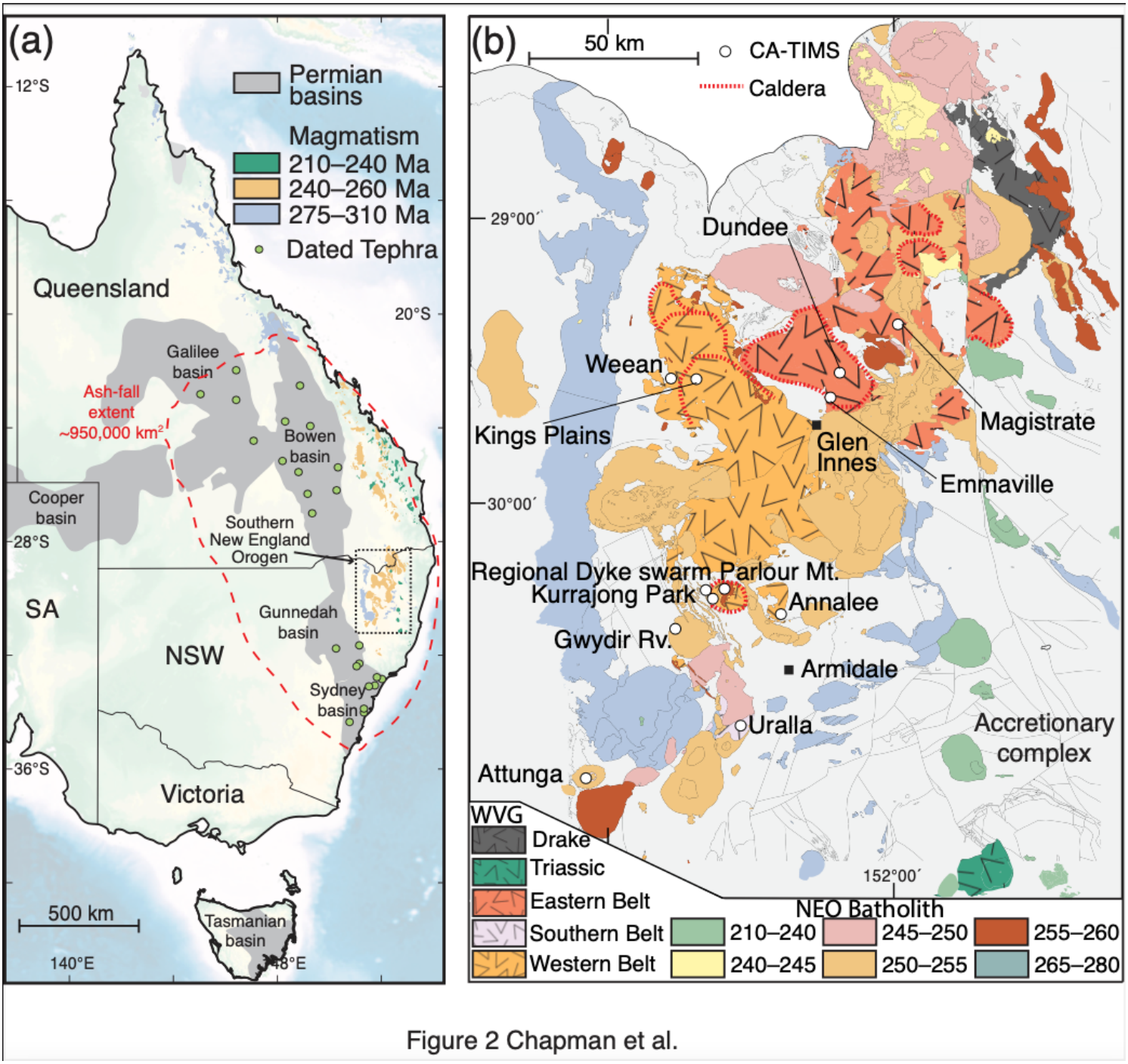

Figure 2 Chapman et al.

Figure 2

Geological maps of eastern Australia Permian–Triassic magmatism including (a) depositional-basins22 with locations of bore holes with published dated tephra (green circles)25,26,31,58. (b) the southern New England Orogen, without Cenozoic cover, displaying locations of CA-TIMS dates from this study (white circles).

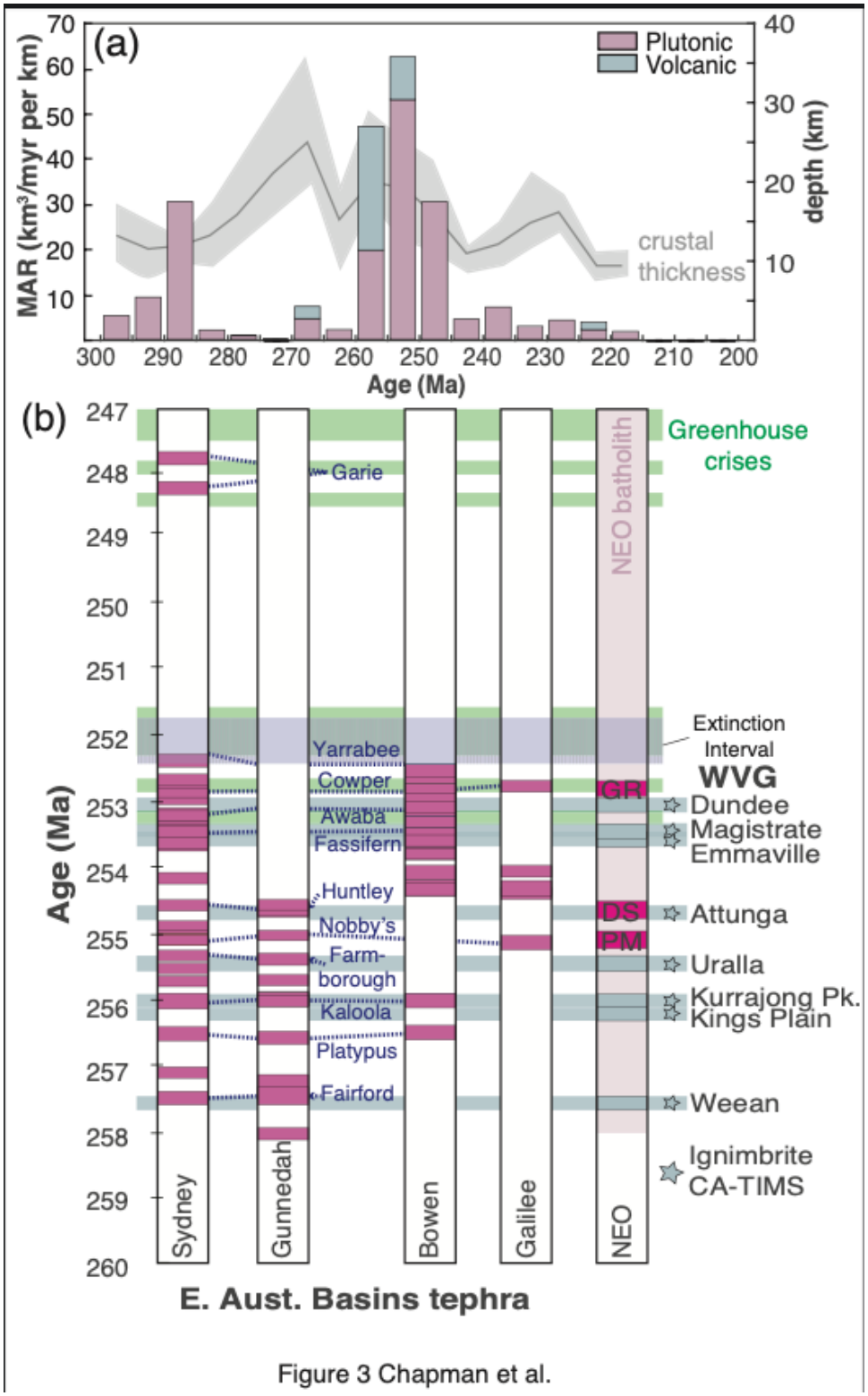

Figure 3

eastern Australia magmatic flare up. (a) Histogram of magma addition rates (MAR in km3/myr per km) along the eastern Australia margin during the Permian–Triassic. (b) Correlation of ignimbrite deposits from the Wandsworth Volcanic Group to published age dates of Tephra in the Sydney, Gunnedah, Bowen and Galilee basins25,26,31,58, and granites in the southern New England Orogen (SNEO: GR = Gwydir River monzogranite; PM = Parlour Mountain leucomonzogranite; DS = Regional Felsic Dyke Swarm).

Identified Eastern Australia greenhouse crises52 are shown with extinction intervals based on floral species47. The thickness of the symbology encompasses the uncertainty on each age date.

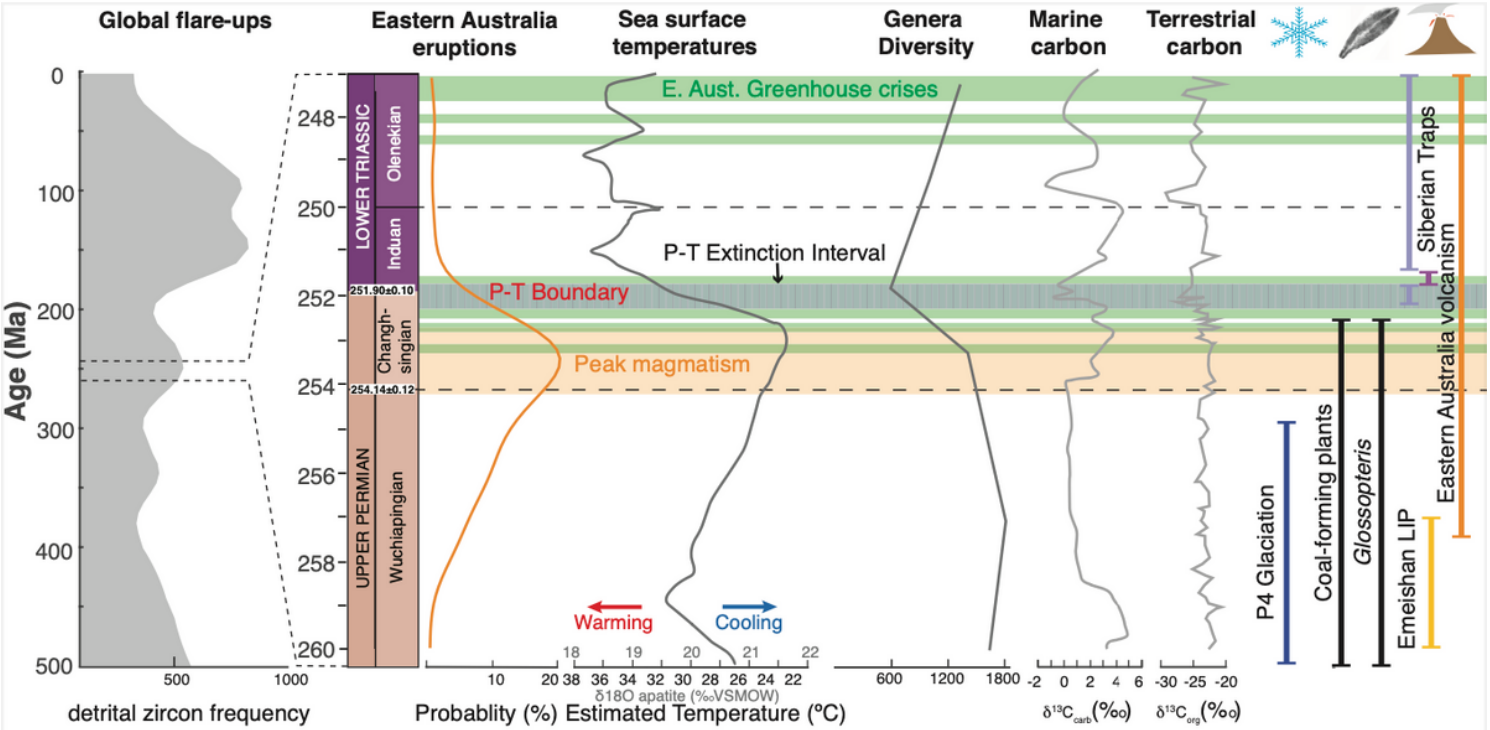

Figure 4 Chapman et al.

Figure 4

Eastern Australia flare-up and the end-Permian mass extinction. The age distribution of volcanism in Eastern Australia at 260–247 Ma in relation to global magma activity based on zircon age systematics59. Identified Eastern Australia greenhouse crises52 are corrected for age systematics25 and associated with floral species demise28,47,48. Carbon isotope curves from marine carbonates in South China43, terrestrial organic material from eastern Australia Basins25, Genera diversity curves from Paleobiology database and sea surface temperature estimates based on conodont Oxygen isotopes37,38,44. The eruption of the Emesishan46 and Siberian Traps and intrusive correlatives3,4 are shown together with the P4 glaciation25.

Supplementary Files

This is a list of supplementary files associated with this preprint. Click to download.

- SupplementaryMethods.docx
- FigS23.pdf
- EAmagmaMapCover.pdf
- NEOLAICPMSdatatable.xls

- NEOCATIMSUPbdatatable.xls